Kinetic pathways of the nematic–isotropic phase transition as studied by confocal microscopy on rod-like viruses

2005 J. Phys.: Condens. Matter 17 S3609

(http://iopscience.iop.org/0953-8984/17/45/055)

INSTITUTE OF PHYSICS PUBLISHING JOURNAL OF PHYSICS: CONDENSED MATTER

J. Phys.: Condens. Matter **17** (2005) S3609–S3618 doi:10.1088/0953-8984/17/45/055

Kinetic pathways of the nematic–isotropic phase transition as studied by confocal microscopy on rod-like viruses

M Paul Lettinga[1], **Kyongok Kang**[1], **Arnout Imhof**[2], **Didi Derks**[2] **and Jan K G Dhont**[1]

[1] IFF, Institut Weiche Materie, Forschungszentrum Jülich, D-52425 Jülich, Germany
[2] Soft Condensed Matter, Debye Institute, Utrecht University, Princetonplein 5, 3584 CC Utrecht, The Netherlands

E-mail: p.lettinga@fz-juelich.de

Received 28 September 2005
Published 28 October 2005
Online at stacks.iop.org/JPhysCM/17/S3609

Abstract

We investigate the kinetics of phase separation for a mixture of rod-like viruses (*fd*) and polymer (dextran), which effectively constitutes a system of attractive rods. This dispersion is quenched from a flow-induced fully nematic state into the region where the nematic and the isotropic phase coexist. We show experimental evidence that the kinetic pathway depends on the overall concentration. When the quench is made at high concentrations, the system is meta-stable and we observe typical nucleation-and-growth. For quenches at low concentration the system is unstable and the system undergoes a spinodal decomposition. At intermediate concentrations we see the transition between both demixing processes, where we locate the spinodal point.

(Some figures in this article are in colour only in the electronic version)

1. Introduction

Systems that are quenched into a state where at least one order parameter is unstable undergo spinodal phase separation. Here, the initially homogeneous system is unstable against fluctuations of arbitrary small amplitude, and phase separation sets in immediately after a quench. In the initial stage of phase separation an interconnected 'labyrinth structure' of regions with somewhat higher and lower values of the order parameter is observed. For quenches where the system becomes meta-stable, phase separation is initiated by fluctuations with a sufficiently large amplitude. Since such fluctuations have a small probability of occurring, phase separation sets in after a certain delay time, referred to as the induction time. Here, nuclei are formed throughout the volume which grow when they are sufficiently large. The

two different mechanisms of phase separation (spinodal decomposition and nucleation-and-growth) can thus be distinguished during the initial stages of phase separation from (i) the difference in morphology (interconnected structures versus growth of isolated nuclei) and (ii) the delay time before phase separation sets in (no delay time for spinodal decomposition and a finite induction time for nucleation-and-growth). As Onsager showed in 1949 [1], the situation is different when the particles are not spherical in shape, i.e. disc-like or elongated particles. Here the system can become unstable or meta-stable with respect to fluctuations in *orientation*. These orientational fluctuations drive concentration differences, resulting in a phase with high concentration and orientational order, the *nematic* phase, and a phase with low concentration and no orientational order, the *isotropic* phase. For very long and thin rods with short-ranged repulsive interactions, the binodal concentrations, i.e. the concentrations of the isotropic and nematic phases in equilibrium after phase separation is completed, have been determined using different approximations in minimizing Onsager's functional for the free energy (see [2] and references therein), while for shorter rods computer simulations have been performed to obtain binodal concentrations [3, 4]. Also the spinodal concentration where the isotropic phase becomes unstable has been found [1, 5].

Binodal points are relatively easy to determine experimentally, since they are given by the concentrations of the bottom and top phase after phase separation. In contrast, it is not at all straightforward to obtain spinodal points, since one would ideally like to perform a concentration quench from low or high concentration into the two-phase region, where the initial state is isotropic or nematic, respectively. In a recent paper a 'quench' of this kind was performed by inducing polymerization of short actin chains [6], and tactoids and spinodal structures were observed. Signatures of spinodal decomposition have also been obtained for boehmite rods, by homogenizing a phase separated system and using sequential polarization microscopy and small angle light scattering measurements [7]. Alternatively, external fields like shear flow [8] and a magnetic field [9, 10] can be applied to prevent a system from phase separation and to stabilize the nematic phase. After cessation of such an external field the nematic phase will become unstable or meta-stable, depending on the constitution of the sample, and phase separation sets in. In this paper we induce a fully nematic phase with a well defined director by imposing shear flow to a dispersion of colloidal rods. We use *fd*-viruses as the system, since the equilibrium phase behaviour concerning the binodal points has been well understood on the basis of Onsager theory [11, 12]. Polymer is added to the dispersion in order to widen the region of isotropic–nematic phase coexistence, which facilitates the phase separation experiments [13]. We perform quenches of a flow aligned initial state to zero shear, which renders the system unstable or meta-stable to fluctuations in the orientation, depending on the concentration of rods. As a consequence phase separation sets in, which we observe by confocal scanning laser microscopy (CSLM). We perform this experiment for different concentrations, throughout the region of phase coexistence. Our results illustrate the difference between nucleation-and-growth and spinodal decomposition in the case of demixing elongated particles, and result in the determination of the nematic–isotropic spinodal point.

2. On the instability of initial states

A convenient way to analyse the stability of a homogeneous initial state is to derive an equation of motion for the order parameter tensor,

$$\mathbf{S}_0(t) = \oint \mathrm{d}\hat{\mathbf{u}}\, \hat{\mathbf{u}}\hat{\mathbf{u}} P_0(\hat{\mathbf{u}}, t). \tag{1}$$

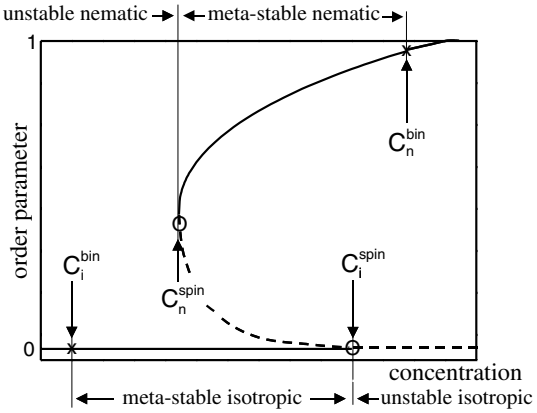

Figure 1. The bifurcation diagram, where the orientational order parameter P_2 is plotted against concentration. Indicated are the various meta- or unstable regions for the two different initial states of the homogeneous suspension. The points marked by X and O are spinodal and binodal points, respectively.

The largest eigenvalue P_2 of the tensor $\mathbf{Q}_0(t) = \frac{3}{2}[\mathbf{S}_0(t) - \frac{1}{3}\hat{\mathbf{I}}]$ (where $\hat{\mathbf{I}}$ is the identity) measures the degree of alignment. For the isotropic state $P_2 = 0$, while for a perfectly aligned state $P_2 = 1$. A stability analysis of stationary solutions of this equation of motion is most conveniently made on the basis of a bifurcation diagram [5], where P_2 for stationary solutions is plotted against the concentration. A schematic bifurcation diagram is given in figure 1. The two solid lines represent stable stationary solutions of the equation of motion, while the dotted lines represent unstable stationary solutions. The isotropic state ceases to be stable above the concentration indicated as C_i^{spin}, while the nematic state becomes unstable at concentrations lower than C_n^{spin}. Above C_i^{spin}, the isotropic state is still a stationary solution, but is now unstable. Below C_n^{spin}, in contrast, there is no unstable nematic state that is a stationary solution of the equation of motion. The two spinodal concentrations C_i^{spin} and C_n^{spin} are connected by a separatrix which separates the basins of attraction for the isotropic and nematic state. A homogeneous initial state above this separatrix develops a higher degree of alignment, while an initial state below the separatrix becomes more isotropic.

Note that the bifurcation diagram relates to homogeneous systems. In an experiment, starting from a homogeneous state, inhomogeneities develop simultaneously with the change of the order parameter of the otherwise homogeneous system. In equilibrium, after completion of phase separation, there is an isotropic phase with concentration C_i^{bin} in coexistence with a nematic phase with concentration C_n^{bin}. One can either start from a stationary state, in which case P_0 in equation (1) is independent of time, or from a non-stationary state, like a nematic state with a concentration lower than C_n, in which case the time dependence of the temporal evolution of alignment of the otherwise homogeneous system couples to the evolution of inhomogeneities through the time dependence of P_0.

In this paper we prepare an initial nematic state shearing a suspension at large enough shear rate such that the induced nematic phase is stable against phase separation (see [14] for a discussion of the bifurcation diagram for sheared systems), and then quench to zero shear rate. For this initial state it is expected that spinodal decomposition occurs at lower concentrations, while nucleation and growth is observed at higher concentrations. For an isotropic initial state this would be reversed: spinodal decomposition at high concentrations and nucleation

Table 1. Overview of the samples used.

Code	$\varphi^5_{\rm nem}$	$\varphi^4_{\rm nem}$	$\varphi^3_{\rm nem}$	$\varphi^2_{\rm nem}$	$\varphi^1_{\rm nem}$
fd (mg ml^{-1})	29.5	28.1	25.8	23.6	19.3
$\varphi_{\rm nem}$	0.96	0.85	0.68	0.52	0.18

and growth at lower concentrations. The observed phase separation kinetics thus depends crucially on the preparation of the initial state of the suspension.

3. Materials and methods

As model colloidal rods we use *fd*-virus particles which were grown as described elsewhere [13]. A homogeneous solution of 22.0 mg ml^{-1} *fd*-virus and 12.1 mg ml^{-1} of Dextran (507 kd, Sigma-Aldrich) in 20 mM tris buffer at pH 8.15 with 100 mM NaCl is allowed to macroscopically phase separate. This concentration of *fd*-virus is exactly in the biphasic region, which is very small when no polymer is added, namely between 21 and 23 mg ml^{-1}. Due to the added polymer, the binodal points shift to 17 and 30 mg ml^{-1}, respectively. New dispersions are prepared by mixing a known volume of the coexisting isotropic and nematic bulk phases. The relative volume of nematic phase in this new dispersion is denoted as $\varphi_{\rm nem}$.

For the microscopic observations we used a home-built counter-rotating coneplate shear cell, placed on top of a Leica TCS-SP2 inverted confocal microscope. This cell has a plane of zero velocity in which objects remain stationary with respect to the microscope while shearing. For details of the setup we refer to [15]. For the measurements described here we used confocal reflection mode at a wavelength of 488 nm. Quench experiments were done as follows. Samples were first sheared at a high rate of 10 s^{-1} for several minutes. The shear was then suddenly stopped, after which images were recorded at regular time intervals. These images were parallel to the flow–vorticity plane. Table 1 gives an overview of the concentrations where quench experiments have been performed.

4. Results

In the top row of figure 2 we show micrographs of the initial stage of phase separation for five different concentrations taken after a shear rate quench from a high shear rate, where the nematic state is stable for each concentration, to zero shear. These images show the flow (vertical)–vorticity (horizontal) plane at a given time after the quench. Thus the director of the initial nematic phase lies in the vertical direction. Fourier transforms of the images are plotted in the second row of figure 2. The background is corrected for by subtracting the Fourier transform of the first frame. The third row plots the development of the total intensity of the images minus the intensity in the isotropic phase, as determined from an isolated isotropic region, normalized by the initial nematic intensity. Qualitatively the difference between the concentrations is obvious. In the first two images, i.e. the two highest concentrations, isolated dark ellipsoidal structures can be seen on a bright background. These are droplets of the isotropic phase referred to as tactoids. The number of tactoids increases when the concentration is decreased ((b) and (c)) until the structures become interconnected ((d) and (e)). This also follows from the Fourier transform of the pictures where a ring is detected for the lowest concentration and a constant increasing intensity towards $K = 0$ for the highest concentration. The timescale at which the inhomogeneities are formed also changes. As can be seen in the third row of figure 2, the high concentrations all show an induction time before the phase separation sets in, while

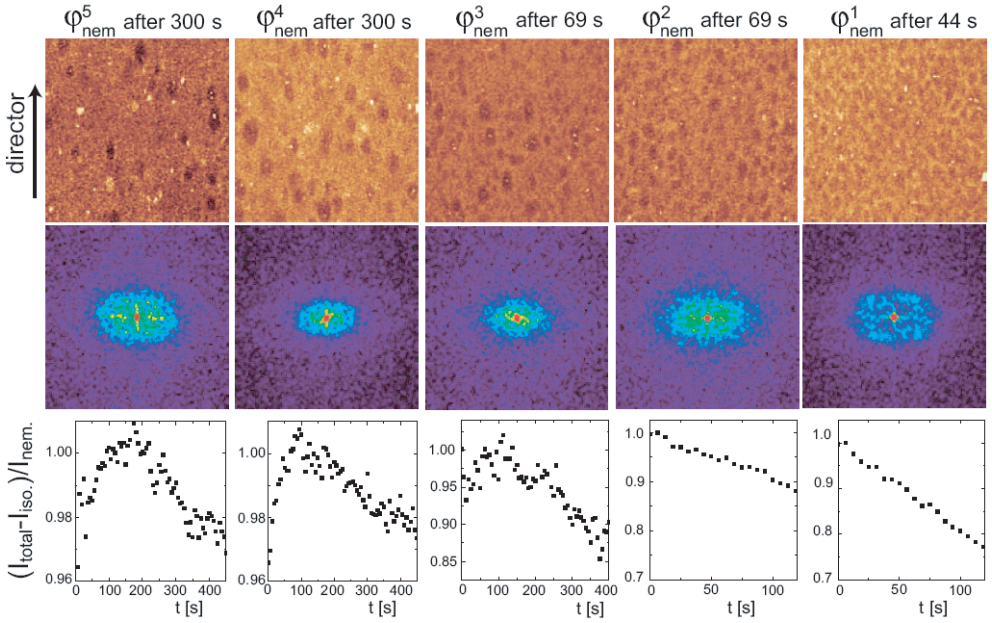

Figure 2. The initial stages of phase separation for five different concentrations after a quench from a flow aligned nematic phase to zero shear. The top row shows the micrographs taken by reflection confocal scanning laser microscopy (field of view = 110 μm); the middle row shows the Fourier transform of the micrographs; the bottom row plots the mean intensity of the micrographs minus the mean intensity for the isotropic phase, normalized by the initial intensity of the nematic phase.

for the low concentrations phase separation sets in immediately. Note also the times at which the images in figure 2 were taken. The isolated nuclei and the induction time are typical for nucleation-and-growth, while the interconnected structures and immediate phase separation are typical for spinodal decomposition.

We use the Fourier transform of the images as shown in figure 2 to quantify the phase separation processes. The interesting quantity for nucleation-and-growth is the width of the Fourier transform, Δk, which is a measure for the anisotropic form factor of the nuclei. Alternatively one could determine the average size of the features in real space, but due to the low contrast this is difficult. For spinodal decomposition the interesting quantity is the wavevector at which the Fourier transform reaches its maximum, $k_{\max}$, quantifying the fastest growing concentration fluctuation. In both cases the fit of the Fourier transform should be performed in two dimensions, since the initial state is anisotropic. Therefore we took cross sections parallel and perpendicular to the director in the Fourier domain, i.e. the vertical and horizontal in figure 2 middle row, to determine $k_{\max}$. Typical cross sections are shown in figure 3, where the wavevector k is scaled by the rod length L. To determine Δk, we performed a 2D Gaussian fit around the origin of the Fourier transforms. Results of a 2D Gaussian fit of the Fourier transform around the origin are shown for the higher concentrations in figures 4(a) and (b), plotting the width in the direction of the director and perpendicular to the director, respectively. $k_{\max}$ as found from fits of the cross sections parallel and perpendicular to the director are given in figures 4(c) and (d), respectively. Both fit procedures result in an anisotropic morphology as can be seen in figure 5, where we plotted $\Delta k_\perp L/\Delta k_\parallel L$ and $k_{\max,\perp} L/k_{\max,\parallel} L$.

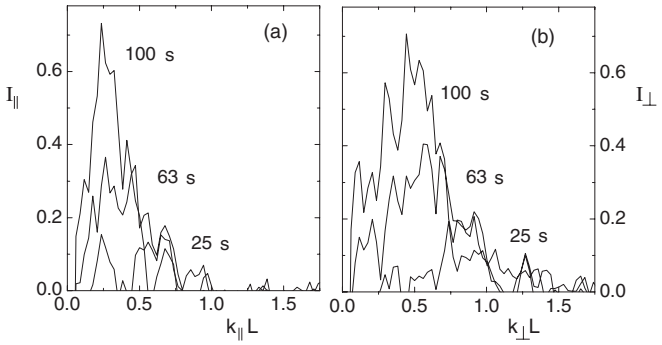

Figure 3. The cross section of the Fourier transform parallel (a) and perpendicular (b) to the director for $\varphi^1_{\rm nem}$. The length is scaled by the rod length L.

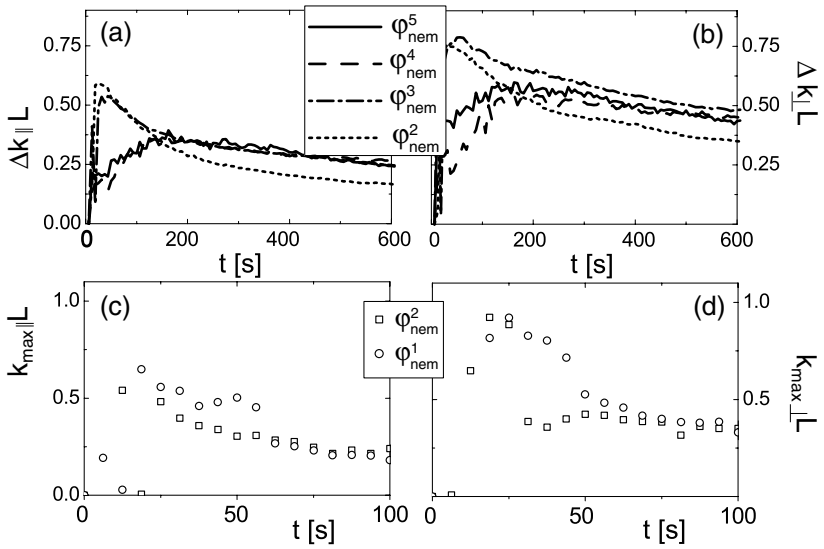

Figure 4. Width of the 2D Gaussian fit, ΔkL, of the Fourier transform parallel (a) and perpendicular (b) to the director for the higher concentrations. Wavevector $k_{\max} L$ where the intensity is maximum for the cross sections parallel (c) and perpendicular (b) to the director for the lower concentrations.

The late stages of the different phase separation processes also show some interesting phenomenology, as can be seen in figure 6. For spinodal decomposition we observe first a growing of the interconnected structures, which then break down into tactoids. Later on the tactoids coalesce, and they become more spherical with increasing size. Note that these tactoids contain the nematic phase and not the isotropic phase, as observed for the nucleation-and-growth process at higher concentrations. In the late stage of nucleation-and-growth, i.e. at high concentrations, we see that coalescence of tactoids containing the isotropic phase as shown in the bottom row of figure 6 is favorable when two tactoids meet somewhat from the middle. In this case the rod orientation near both features is similar and the barrier which has to be overcome for coalescence is low.

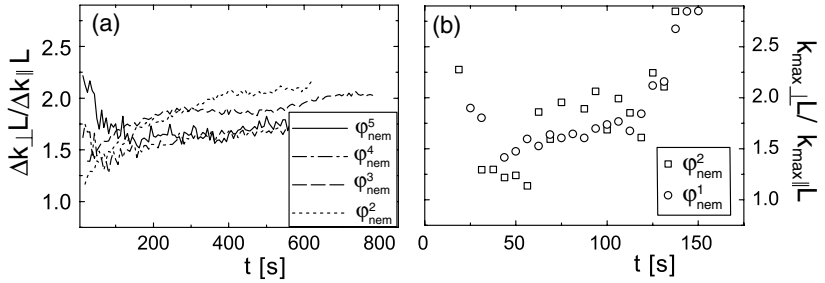

Figure 5. (a) The ratio $\Delta k_\perp L/\Delta k_\parallel L$ for the higher concentrations and (b) the ratio $k_{\max,\perp}L/k_{\max,\parallel}L$ for the lower concentrations.

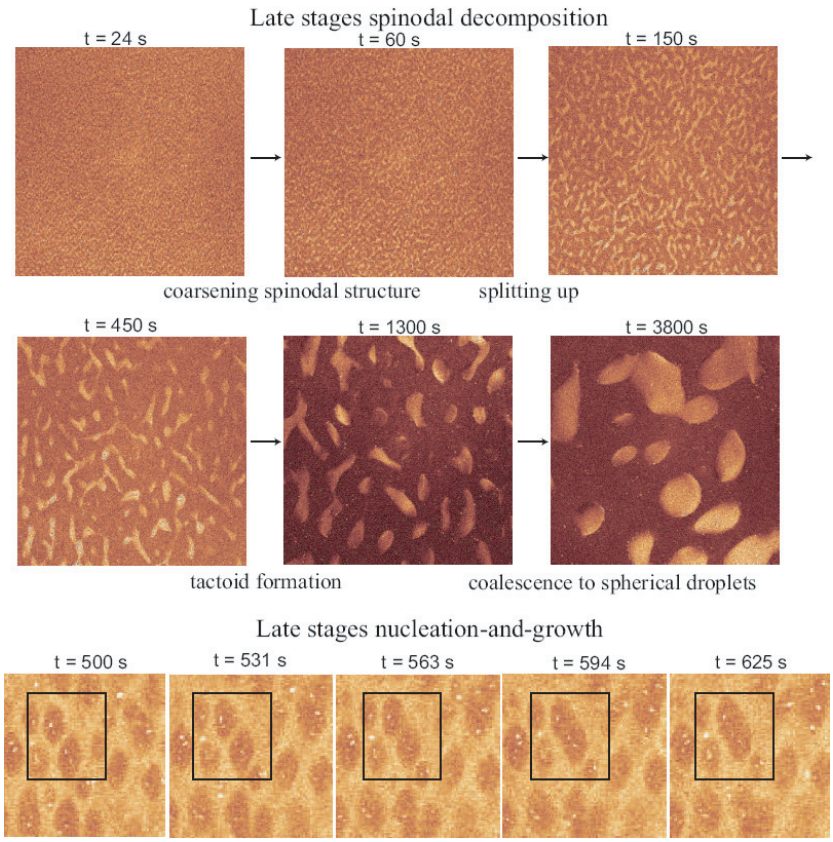

Figure 6. The late stages for spinodal decomposition in the top two rows (φ^1_{nem}, field of view = 375 μm), and coalescence of tactoids in the bottom row (φ^5_{nem}, field of view = 73 μm).

5. Discussion

On the basis of these observations we can now locate the metastable region, i.e. where the system has to overcome a free energy barrier, and the unstable region, where there is no such barrier. At the high concentrations (φ^5_{nem}, φ^4_{nem}) the system is meta-stable, which is reflected by the observed isolated structures formed (top row in figure 2) and the induction time (bottom

row in figure 2). With decreasing concentration the system approaches the unstable region: the number of nuclei increases while the induction time decreases and finally vanishes. The lowest concentration $\varphi^1_{\rm nem}$ is clearly unstable after cessation of the flow. It shows all the features typical for spinodal decomposition: phase separation immediately sets in throughout the whole sample, with a typical length scale which is characterized by the scattering ring observed in the Fourier transform. It can be shown, in fact, that the observed phase separation process for the lowest concentration has features typical for the spinodal decomposition of rods, as derived recently from a microscopic theory by one of the authors [16]. This will be the subject of a following paper [17].

In the intermediate region it is difficult to judge from the morphology if nucleation-and-growth takes place or spinodal decomposition, since it is difficult to distinguish between a high number of tactoids and an interconnected structure. However, $\varphi^3_{\rm nem}$ shows a short induction time after the quench after which clearly separated tactoids are formed, while for $\varphi^2_{\rm nem}$ phase separation immediately sets in showing ellipsoidal structures which clearly 'influence' each other. Moreover, figure 4 shows that the size of the structures formed in $\varphi^3_{\rm nem}$ coincides after some time with the clearly nucleated structures of $\varphi^4_{\rm nem}$ and $\varphi^5_{\rm nem}$, while the size of the structures formed in $\varphi^2_{\rm nem}$ coincides with samples which clearly show spinodal decomposition. Thus, we locate the transition from meta-stable to unstable, i.e. the spinodal point, between at 23.5 and 25.8 mg ml^{-1}. This is the first experimental observation of the spinodal point in a rod-like system. We should mention at this point that in fact our sample consists of a mixture of rods and polymer. Addition of the polymer causes a widening of the biphasic region [13], i.e. a shift of the binodal points. It is now interesting to see that the high concentration binodal shifts as much as from 23 to 30 mg ml^{-1}. In contrast, the high concentration binodal point, $C_n^{\rm bin}$, shifts from a concentration between 21 and 23 mg ml^{-1} to somewhere between 23.5 and 25.8 mg ml^{-1}. This leads to the interesting conclusion that the shift of the high concentration binodal point, $C_n^{\rm bin}$, due to the attraction between the rods, is considerable compared to the shift of the high concentration spinodal point, $C_n^{\rm spin}$. In other words, making the rods attractive causes a widening of the meta-stable region, while the unstable region remains unaffected. Addition of more polymer will result in more complex kinetics as described in [18].

Interestingly, for all concentrations we observe that the morphology of the phase separating system is anisotropic. This is most clear for the highest concentrations, where the tactoids all point upwards, i.e. in the direction of the director of the surrounding nematic phase. Also the Fourier transforms for the lower concentrations show deformed intensity rings in Fourier space (rightmost FFT image in figure 2). Moreover, the kinetics of the phase separation is also fastest in the direction of the nematic director. This follows for instance from the ratio of $\mathbf{k}_{\rm max}$ as plotted in figure 5(b), which increases in time. In other words, for all concentrations phase separation is anisotropic, due to residual alignment after the quench of the initially strongly sheared suspension, and not isotropic as is the case for spheres [19].

The length of the first observed tactoids just below $C_n^{\rm bin}$ is about 12 times the rod length, while just above $C_n^{\rm spin}$ it is seven times the rod length. The thickness is about two-thirds of the length in both cases. Typical length scales for the initial spinodal morphology are not more than six rod lengths. These sizes seem to be quite small, considering also the random orientation of the rods in the isotropic phase, but it is in accordance with the microscopic theory for spinodal decomposition of rods [16]. It does suggest that we really image the initial stage. The breaking up of the spinodal structure into nematic tactoids and the sequential growth in the late stage of spinodal decomposition seems surprising since for dispersions of spheres only coalescence and macroscopic phase separation would be observed. However, a similar order of events has been observed for polymer mixtures with thermotropic liquid crystals [20]. Simulations on

such mixtures show that the breakdown is due to the effect of the flow-alignment coupling, and not primarily due to elastic effects [21]. An explanation along the same lines was given by Fukuda in a numerical treatment of time-dependent Ginzburg–Landau equations of liquid crystalline polymers [22]. The volume dependence of the morphology in the final stage can be explained by the competition between the interfacial tension and nematic elasticity of the tactoids [23].

6. Conclusion

We studied the kinetics of the nematic–isotropic phase transition of a dispersion of *fd*-virus particles with added polymer after shear quenches into the two-phase region. By varying the equilibrium rod concentration φ_{nem} we were able to detect a nucleation-and-growth mechanism for high φ_{nem}, spinodal decomposition for low φ_{nem}, and the transition between the two processes. In this way we were able to trace for the first time the nematic–isotropic spinodal point C_n^{spin}. Thus, we found that addition of polymer widens the meta-stable region greatly. Furthermore, we showed that the phase separation is strongly influenced by the director of the initial nematic state. The nematic phase also influences the late stages of spinodal decomposition, causing a splitting up of the interconnected structures.

Acknowledgment

This work was performed within the framework of the Transregio SFB TR6, 'Physics of colloidal dispersions in external fields'.

References

[1] Onsager L 1949 The effect of shape on the interaction of colloidal particles *Ann. New York Acad. Sci.* **51** 627–59
[2] Vroege G J and Lekkerkerker H N W 1992 Phase transitions in lyotropic colloidal and polymer liquid crystals *Rep. Prog. Phys.* **55** 1241–309
[3] Bolhuis P and Frenkel D 1997 Tracing the phase boundaries of hard spherocylinders *J. Chem. Phys.* **106** 666–87
[4] Graf H and Löwen H 1999 Phase diagram of tobacco mosaic virus solutions *Phys. Rev.* E **59** 1932–42
[5] Kayser R F Jr and Raveché H J 1978 Bifurcation in Onsager's model of the isotropic–nematic transition *Phys. Rev.* A **17** 2067–72
[6] Viamontes J and Tang J X 2005 Formation of nematic liquid crystalline phase of f-actin varies from continuous to biphasic transition http://arxiv.org/abs/cond-mat/0506813
[7] van Bruggen M P B, Dhont J K G and Lekkerkerker H N W 1999 Morphology and kinetics of the isotropic–nematic phase transition in dispersions of hard rods *Macromolecules* **32** 2256–64
[8] Lenstra T A J, Dogic Z and Dhont J K G 2001 Shear-induced displacement of isotropic–nematic spinodals *J. Chem. Phys.* **114** 10151–62
[9] Tang J and Fraden S 1993 Magnetic-field-induced phase transition in a colloidal suspension *Phys. Rev. Lett.* **71** 3509–12
[10] Lemaire B J, Davidson P, Ferré J, Jamet J-P, Petermann D, Panine P, Dozov I, Stoenescuc D and Jolivet J-P 2005 The complex phase behaviour of suspensions of goethite (α-FeOOH) nanorods in a magnetic field *Faraday Discuss.* **128** 271–83
[11] Fraden S 1995 *Observation, Prediction, and Simulation of Phase Transitions in Complex Fluids* (*NATO-ASI-Series* C, vol 460) ed M Baus, L F Rull and J P Ryckaert (Dordrecht: Kluwer–Academic) pp 113–64
[12] Chen Z Y 1993 Nematic ordering in semiflexible polymer chains *Macromolecules* **26** 3419–23
[13] Dogic Z, Purdy K R, Grelet E, Adams M and Fraden S 2004 Isotropic–nematic phase transition in suspensions of filamentous virus and dextran *Phys. Rev.* E **69** 051702
[14] Dhont J K G and Briels W J 2003 Viscoelasticity of suspensions of long, rigid rods *Colloids Surf.* A **213** 131–56
[15] Derks D, Wisman H, van Blaaderen A and Imhof A 2004 Confocal microscopy of colloidal dispersions in shear flow using a counter-rotating coneplate shear cell *J. Phys.: Condens. Matter* **16** S3917–27
[16] Dhont J K G and Briels W J 2005 Isotropic–nematic spinodal decomposition kinetics *Phys. Rev.* E at press

[17] Lettinga M P, Kang K, Holqvist P, Imhof A, Derks D and Dhont J K G 2005 Nematic–isotropic spinodal decomposition of rod-like viruses, submitted
[18] Dogic Z 2003 Surface freezing and a two-step pathway of the isotropic–smectic phase transition in colloidal rods *Phys. Rev. Lett.* **91** 165701
[19] Aarts D G A L and Lekkerkerker H N W 2004 Confocal scanning laser microscopy on fluid–fluid demixing colloid–polymer mixtures *J. Phys.: Condens. Matter* **16** S4231
[20] Nakai A, Shiwaku T, Wang W, Hasegawa H and Hashimoto T 1996 Process and mechanism of phase separation in polymer mixtures with a thermotropic liquid crystalline copolyester as one component *Macromolecules* **29** 5990–6001
[21] Araki T and Tanaka H 2004 Nematohydrodynamic effects on the phase separation of a symmetric mixture of an isotropic liquid and a liquid crystal *Phys. Rev. Lett.* **93** 015702
[22] Fukuda J 1999 Phase separation kinetics of liquid crystalline polymers: effect of orientational order *Phys. Rev.* E **59** 3275–88
[23] Prinsen P and van der Schoot P 2003 Shape and director-field transformation of tactoids *Phys. Rev.* E **68** 021701